



Detection of shockable ventricular arrhythmia using optimal orthogonal wavelet filters

Manish Sharma¹ · Ru-San Tan² · U. Rajendra Acharya^{3,4,5}

Received: 13 October 2018 / Accepted: 23 January 2019 / Published online: 13 February 2019
© Springer-Verlag London Ltd., part of Springer Nature 2019

Abstract

Sudden cardiac death (SCD) is caused by lethal arrhythmia. Ventricular fibrillation (VF) and ventricular tachycardia (VT) are amenable to defibrillation or electrical shock therapy (“shockable” arrhythmia) that can abolish the VF/VT and restore normal electrical and mechanical heart function. The challenge is to differentiate between shockable and non-shockable arrhythmia during the emergency response to SCD. When it comes to saving the life, accurate electrocardiogram (ECG) diagnosis and fast delivery of appropriate treatment is imperative. Automated systems to differentiate shockable from non-shockable arrhythmia have been developed to overcome the difficulty, and possible errors due to the manual inspection. In the present work, we have devised an efficient, effective and robust automated system to detect shockable and non-shockable arrhythmia using an optimal wavelet-based features extracted from ECG epochs of 2 s durations. We employed optimal two-channel frequency selective orthogonal wavelet filter bank to diagnose shockable ventricular arrhythmia. The optimization was carried out by minimizing the stop band ripple energy of the wavelet filter. The optimal orthogonal wavelet filter has been designed using a semi-definite programming (SDP) formulation without the use of any parameterization. The SDP solution gave us the desired optimal orthogonal wavelet filter bank with minimum stop band energy and the desired degree of regularity for the given length of filter. Fuzzy entropy and Renyi entropy features were extracted from the 2-s ECG epochs. These extracted features were then fed into the classifiers for discrimination of shockable arrhythmia rhythms and non-shockable arrhythmia rhythms. The best results were obtained from support vector machine. Accuracy of 97.8%, sensitivity of 93.42%, and specificity of 98.35% were obtained using a tenfold cross validation scheme. The developed automated system is accurate and robust; therefore, it can be integrated in automated external defibrillators that can be deployed for hospitals as well as out-of-hospital emergency resuscitation of SCD.

Keywords Electrocardiogram ECG · Shockable rhythms · Non-shockable rhythms · Biorthogonal filter bank · Stopband energy · SVM

1 Introduction

Sudden cardiac death (SCD) or cardiac arrest refers to a situation where the heart stops pumping, which leads either to death or, frequent devastating neurological deficits among hospitalized survivors. SCD can be the result of a heart attack, where sudden blockage in coronary arterial blood flow to the heart depletes heart muscle oxygen levels precipitately, triggering off an arrhythmia that embarrasses heart muscle contraction [18]. Alternatively, congenital or acquired defects in the electrical conduction system within the heart can initiate potentially lethal arrhythmia. The majority of SCD occur out of hospital, with death often occurring within minutes of presentation. There exists only a very narrow time window for the emergency response

✉ Manish Sharma
manishsharma@iitram.ac.in

¹ Department of Electrical Engineering, Institute of Infrastructure, Technology, Research and Management (IITRAM), Ahmedabad 380026, India

² National Heart Centre Singapore, Singapore, Singapore

³ Nagee Department of Electronics and Computer Engineering, Ngee Ann Polytechnic, Singapore 599489, Singapore

⁴ Department of Biomedical Engineering, School of Science and Technology, SUSS University, Singapore, Singapore

⁵ Department of Biomedical Engineering, Faculty of Engineering, University of Malaya, Kuala Lumpur, Malaysia

team to arrive and deliver treatment of electrical cardioversion (or shock) using defibrillators, followed by cardiopulmonary resuscitation and/or drugs where appropriate—to terminate the arrhythmia and avert death. Deaths due to SCD accounts for more than three hundred thousand deaths in the United States of America alone every year [31, 42]. It exacts an equally heavy toll in the developing world [20]. In India, it has been reported that 10.3% of total deaths were due to SCD [37]. Electrocardiographic (ECG) diagnosis is crucial for deciding on the appropriate emergency intervention, i.e., whether or not to deliver electrical defibrillation or shock treatment. If there is no electrical activity in the heart (asystole), shock is contraindicated. Pulseless electrical activity (PEA) occurs when the ECG signals are present without any pulse. The ECG rhythm in PEA can either be slow (bradycardia) or fast. Indeed, most SCD is attributable to rapid high grade ventricular arrhythmias, for which electrical shock therapy can be used to terminate the arrhythmia and is potentially life-saving. All external (and implanted) defibrillators are equipped with heart rhythm analysis algorithms to detect lethal ventricular arrhythmia that demands immediate shock—“shockable”. As indiscriminate shocks may induce pain and injure heart muscle, the need for rapid and accurate differentiation between “shockable” (requires defibrillation) and non-shockable arrhythmia (defibrillation is not helpful) is most preferred.

Shockable ventricular arrhythmia comprises ventricular tachycardia (VT) and ventricular flutter (VFL) and the most deadly ventricular fibrillation (VF) [18]. In VF, the ventricles fibrillates, chaotically quivering 400–600 times per minute, result in disorganized intracardiac blood flow and absence of effective heart contraction or output. The ECG shows rapid, irregular and broad QRS complexes. Death ensues within 3–5 min without shock treatment with defibrillators, which terminate VF, restore regular (or sinus) rhythm and synchronized heart contractions which can generate pulsatile cardiac output. VT is more common, accounting for 80% of SCD [31]. VT, like VF, originates in the ventricles from scar tissue due to either prior myocardial infarction or other non-ischemic heart muscle or conductive tissue disease. In VT, the heart beats can beat at a frequency between 110 and 250 bpm. The ECG in VT shows regular rapid QRS complexes. There is variable effect on intracardiac blood flow and cardiac output. In some cases, the pulse may still be present. However, when the victim develops hemodynamic compromise evidenced by sudden drop in blood pressure, loses consciousness due to blood flow to brain, or the pulse becomes undetected (pulseless VT), emergency shock therapy is given. VFL is a regular rapid ventricular rhythm with frequency of 250–350 beats per minute that is intermediate and sometimes transitory between VT and VF.

In general, asystole and bradycardias are non-shockable rhythms. In asystole, there is neither atrial nor ventricular electrical activity (absent P waves and QRS complexes) and the ECG shows a “flat line”. The blood pressure is unrecordable. Use of defibrillators is ineffective in restoring electrical or mechanical heart function. The prognosis for survival is dismal, and more than 85% of resuscitated asystolic victims succumb [30]. Similarly, in pulseless electrical activity (PEA) with bradycardia, even though the heart is electrically active albeit slow, the rate is too slow to sustain meaningful mechanical heart muscle contraction and output. Shock therapy in this case will neither jump-start electrical nor mechanical heart function and may induce heart muscle injury.

The ECG must be able to diagnose shockable and non-shockable arrhythmia attributes, so that appropriate shock is delivered only for the shockable lethal ventricular arrhythmia (VF, VFL and pulseless VT). The continual refinement and optimization of automated algorithms that achieve higher accuracy for discriminating shockable from non-shockable arrhythmias with minimum error is most Desirable. In the literature, several automated systems have been introduced. Various studies have been conducted on the detection and classification of shockable arrhythmia rhythms (SAR) and non-shockable arrhythmia rhythms (NSAR). We have briefly reviewed few existing state-of-algorithms below.

Jekova [25] compared the performance of five previously presented algorithms [8, 13, 29, 61, 71]. Later in 2004, Jekova and Krasteva [27] proposed a simple algorithm for the real-time detection of VT and VF by implementing band-pass digital filter. The complexities and computational costs present in earlier developed algorithms motivated Jekova [26] to work on finding a simple algorithm. They presented a set of ten parameters which were used for the shockable rhythm detection, which can be used for automated external defibrillators (AED).

Amann et al. [7] worked on the time-delay methods for the diagnosis of life-threatening VF. Fokkenrood et al. [19] explored the possibilities of monitoring the heart condition by using blue-tooth enabled sensing devices and smart phones for real-time monitoring of heart functioning and also detection of VT/VF.

Atienza et al. [6] extracted morphological, spectral and complexity features from ECG signals for the automated diagnosis of shockable and non-shockable arrhythmia. They used support vector machine (SVM) for classification and achieved sensitivity (SEN) and specificity (SPE) of 92.0% and 97.0%, respectively. Alonso-Atienza et al. [6] analyzed the findings of several algorithms developed earlier. Thirteen morphological, spectral and complexity features of the ECG were used for the analysis.

Li et al. [32] used VF-filter leakage measure, complexity measure and other statistical features for the classification problem. They achieved a maximum ACC, SEN and SPE of 96.3%, 96.2% and 96.2%, respectively, using SVM.

Tripathy et al. [62] employed variational mode decomposition (VMD) decompose the arrhythmia rhythms into sub-signals and derived energy, Renyi entropy and permutation entropy of these sub-signals. Further, they used random forest (RF) classifier on the extracted features for classification. They achieved ACC of 97.23%, sensitivity (SEN) of 96.54% and specificity (SPE) of 97.97%.

Acharya et al. [2] processed arrhythmia signal using a convolutional neural network (CNN) model. Their CNN model comprised eleven layers and achieved an accuracy (ACC) of 93.18% with a sensitivity of 95.23% and specificity of 91.04%.

As SCD is life-threatening, timely and appropriate emergency intervention mandates accurate diagnosis, i.e., whether the arrhythmia recorded during SCD is shockable or non-shockable. Since wavelet-based features confer good classification performance for physiological signals including ECG signals [10, 46, 52, 54], we have employed optimal orthogonal wavelet filter banks [44] and exploited the wavelet-based features for automated classification of shockable and non-shockable arrhythmia in this study. The objective of this study is twofold. First, we designed an optimal orthogonal wavelet filter banks [56–58]. Secondly, we also aim to develop a robust, efficient and inexpensive computer-aided and efficient classification system for detecting whether the recorded beats are shockable or non-shockable rhythms using the designed wavelet-based features. The system needs to be accurate, robust and reliable. As mentioned above, SCD affects developing countries equally. Hence, the solution should be inexpensive and feasible for implementation in the third-world countries.

2 Methodology

The flow diagram of the proposed study is shown in Fig. 1. In this work, we have used two classes of ECG signals, viz. shockable and non-shockable rhythms. The first step was to filter out noise and make the raw data ready for the analysis. Five level decomposition was carried out on the filtered data to obtain six subbands for each ECG epoch. For this purpose, we used the optimal two-channel frequency selective orthogonal filter bank designed by Karmakar et al. [28]. Extraction of features from the data (subbands) was then performed. The best results were obtained with fuzzy entropy and Renyi entropy. The extracted features were then fed into various supervised machine-learning-based classifiers for the classification of two classes.

3 Material used

The data used in this work were obtained from three databases, viz. MIT-BIH arrhythmia database (MITDB) [21, 33], MITBIH malignant ventricular arrhythmia database (VFDB) [21, 23] and Creighton University ventricular tachyarrhythmia database (CUDB) [21, 36]. The data from MITDB contains forty-eight two-channel ECG signals of duration 30 min, and were resampled at 250 Hz. The MITDB ECG recordings had been annotated using 15 labels including VT, VFL, normal sinus rhythm among others. The data of VFDB had twenty-two two-lead ECG signals of, 35 min duration each, and were sampled at 250 Hz. The data from CUDB comprises of thirty-five single-channel ECG signals of, 8 min duration each, with frequency sampling of 250 Hz. Table 1 presents the summary of the data used in this study. The ECG recordings have been labeled as with-VF and without-VF. Figure 2 shows the ECG signal showing sinus rhythm in a healthy person. Figures 3 and 4 depict non-shockable and shockable ECG signals. We have segmented the collected ECG recordings in to epochs of duration of 2 s each. The SAR ECG epochs

Fig. 1 Proposed methodology for the automated detection of shockable ECG signals

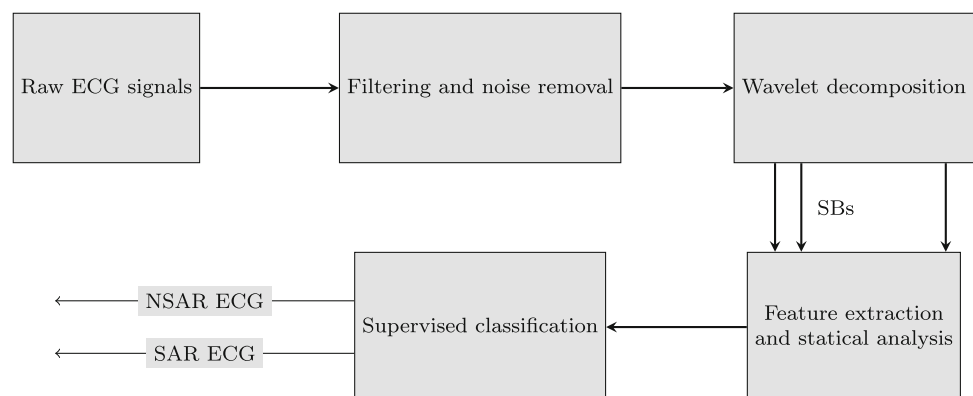
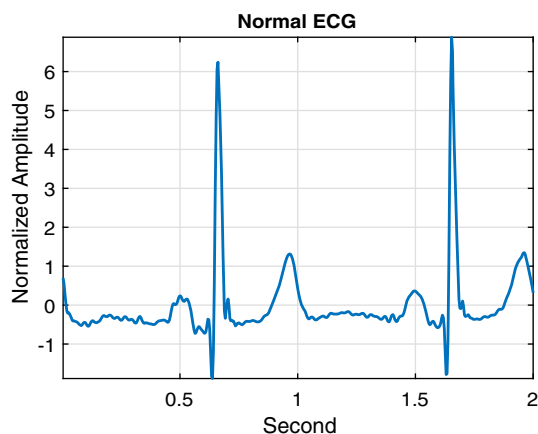
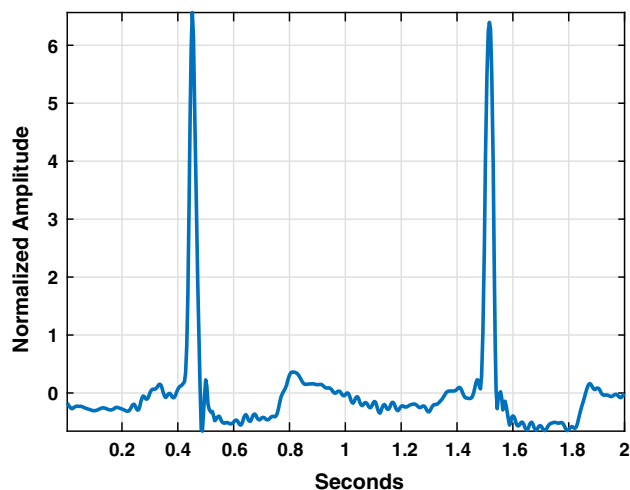
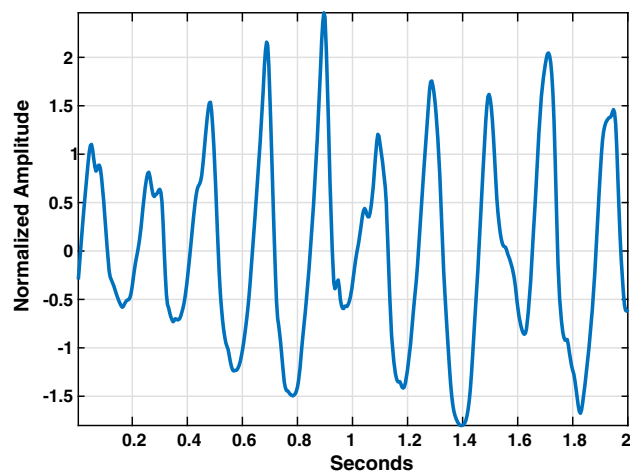


Table 1 Details of the datasets used in the study

Dataset	NoS	Duration (min)	Frequency (Hz)	Leads employed
MITDB	48	30	360	Modified lead-II
VFDB	22	30	250	Lead-I
CBDB	35	8	250	Lead-I

**Fig. 2** Sample normal ECG epoch**Fig. 3** Sample NSAR ECG

belong to either VT ECG episodes or VF/VFL ECG episodes. The NSAR ECG epochs comprise normal sinus rhythm, ventricular bigeminy, ventricular ectopic beats, and ventricular escape rhythm. We considered total 48,095 NSAR and 6001 SAR ECG epochs in this work.

**Fig. 4** Sample SAR ECG

4 Pre-processing

Raw ECG databases are pre-processed before applying to the system. The raw ECG signals were pre-processed using the wavelet-based filtering used in [2]. We have used orthogonal wavelet filter of length-12 with six vanishing moments [15] which helps to remove the baseline wander and noise. Then, filtered ECG signals are windowed and labeled as NSAR and SAR as per annotations provided in the respective databases. Each windowed ECG epoch is of duration 2 s which contains five hundred samples. The ECG epochs so obtained are normalized using Z-score test.

5 Wavelet filter banks for ECG analysis

Due to the non-stationary nature of ECG signals, Fourier transform-based techniques fail to analyze the ECG signals. Wavelet bases have been found to be efficient to analyze the non-stationary ECG signal [55, 63]. Many researches have employed discrete wavelet transform (DWT) for the analysis of ECG signals. Mostly, Daubechies orthogonal wavelet filters [15] have been employed to analyze the ECG signals. Several classes of wavelet filters have been employed to analyze the non-stationary signals [64]. The choice of a particular wavelet filter depends upon the given application, and the type of the signal to be analyzed. Daubechies orthogonal wavelet filters cannot be considered as the best choice in every application, although they have the maximum smoothness or regularity. Various optimality criteria [11] have been used to design optimal wavelet filter banks. Optimal filter wavelet filter banks have been designed to analyze the signals accurately [53, 59]. To design optimal filters either ripple energies or maximum ripples in the passband and stopband are to be minimized [16, 35]. In this study, we

used optimal wavelet filters obtained by minimizing the ripple energy in the stopband [28].

We have worked using the optimal two-channel frequency selective orthogonal filter bank [28]. The wavelet filter bank used in this study belongs to an optimal class of orthogonal filter bank. There have been several attempts to classify the bio-signals by applying orthogonal filter banks [12, 15, 50]. The dyadic wavelets are generated by the iteration of perfect reconstruction (PR) two-channel filter bank. In a two-channel PR filter bank, the input signal is first fed into its high-pass and low-pass components and then down sampled by a factor of two. The analysis part of the filter bank breaks down the input signal, while the synthesis side reconstructs the signal using extrapolation. The limitation of widely used Daubechies orthogonal filter banks [15] is that they do not facilitate any freedom for optimizing desired attributes of the filter. This is because they are obtained from the factorization of Lagrange half-band polynomial possessing maximum possible zero moments (ZM) [53]. Thus, one has no freedom to design an optimal filter. But, in practice, we need freedom to set the desired characteristics of the filter, and for this purpose, we adjust few of ZMs. Suitable filter bank is obtained by setting the characteristics such as stopband energy, energy-compaction, smoothness and bandwidth-duration concentration appropriately [49]. Often, an optimal filter is obtained by minimizing either energy in the stopband or the highest ripples in the stopband and passbands [49].

It is worth noting that Sharma et al. [47, 60] have used wavelet-based features for ECG analysis. However, in those work, they have not attempted to detect SAR using the wavelet-based features. This is the first time; we use optimal wavelet-based features for detection of SAR. Further, in the previous work, Sharma et al. [47, 60] have designed optimal biorthogonal wavelet filter banks considering joint duration-bandwidth concentration as an optimality c -measure. However, the proposed work employ optimum orthogonal filter banks which have been designed considering stop band ripple energy as our designing criterion. Further, to design, we use semi-definite programming (SDP) for obtaining the best filters, whereas Sharma et al. [47, 60] have used eigenvalue based and some other convex optimization techniques to obtain optimal filters.

In the proposed study, we aim to get a low-pass filter that has the least stopband ripple energy for the underlying two-band orthogonal wavelet filter bank and to judge the efficacy of the optimum filter in SAR detection. The construction of filter bank has been transformed to a semi-definite programming (SDP) optimization problem [48]. The solution to this SDP will provide us with the desired filter bank. Also, the filter bank is designed so as to have the required number of ZMs and with minimum phase [49]. The SDP gives us the coefficients of the filter in the time

domain directly, without implementing any parametrization technique [46].

5.1 Optimal filter bank design

The analysis part of the two-channel filter bank comprises a scaling filter $C(z)$ and wavelet filter $\tilde{C}(z)$, both followed by a downsampler which down samples the output of the filter by a factor of 2. And the synthesis filter bank contains a scaling filter $D(z)$ and a wavelet filter $\tilde{D}(z)$, each one preceded by upsampler of factor 2. The filters $C(z)$ and $D(z)$ fulfill orthogonality conditions. The orthogonality condition can be related to the product filter $Q(z) = C(z)D(z)$ as given below [51]:

$$Q(z) + Q(-z) = 2 \quad (1)$$

Here $Q(z)$ is the product filter and is defined as:

$$Q(z) = C(z)D(z) = C(z)C(z^{-1}) \quad (2)$$

The product filter's the frequency response satisfies the following non-negativity condition [15]:

$$Q(e^{j\omega}) = |C(e^{j\omega})|^2 \geq 0 \quad (3)$$

For the analysis scaling filter $C(z)$ to have Z th-order regularity, the product filter should have $2Z$ ZMs. The ZMs are zeros of the filter at $z = -1$ [45].

5.2 Proposed optimization technique

In further discussions, $c(n)$ and $d(n)$ represent the impulse responses of respective analysis and synthesis scaling filters. To obtain optimal orthogonal wavelet filter bank, we minimize the stopband energy of the analysis scaling filter $C(z)$. As the filter bank is orthogonal, minimization of stopband energy of $C(z)$ will also give us the synthesis scaling filter $D(z)$ with minimum stopband energy [15]. The stopband energy, E_{sp} , of the filter $C(z)$ for the given stopband edge frequency ω_s is represented by:

$$E_{sp} = \frac{1}{\pi} \int_{\omega_s}^{\pi} |C(e^{j\omega})|^2 d\omega \quad (4)$$

where $C(e^{j\omega})$ is the frequency response of the analysis low-pass filter.

We have transformed filter bank construction problem into constrained optimization problem, wherein our objective is to minimize the stopband energy the scaling filter with the restriction of orthonormality and M -order smoothness. The design problem has been converted to the following optimization problem:

$$\text{minimize}(E_{\text{sp}}) = \frac{1}{\pi} \int_{\omega_s}^{\pi} |C(e^{j\omega})|^2 d\omega \tag{5}$$

subject to

$$\sum_{n=0}^{N-1} c(n)c(n-2k) = \delta(k); \quad k = 0, 1, \dots, (N/2 - 1) \tag{6}$$

$$\sum_{k=0}^{N-1} (-1)^k k^l c(k) = 0; \quad l = 0, 1, \dots, Z - 1 \tag{7}$$

where N is the length of the filter and Z denotes the number of vanishing moments of the filter $C(z)$.

Equation (5) presents the objective function, while Eq. (6) represents double-shift orthogonality constraint and Eq. (7) represents the Z -order regularity constraint. The orthonormality constraints (6) being non-convex lead to a non-convex optimization problem. To convert the non-convex optimization problem into a convex problem, the minimizing function and conditions have been reformulated as functions of the variable $Q(z)$.

The impulse response $q(n)$ of the product filter $Q(z)$ can be related to the impulse response, $c(n)$ of the analysis scaling filter as $q(n) = \sum_k c(k)c(k+n)$. As mentioned in (3), $Q(e^{j\omega}) \geq 0$, hence, the sequence $q(n)$ must be an autocorrelation sequence. In order to satisfy orthogonality conditions, the product filter $Q(z)$ of order $2N - 2$ should have the following form [34],

$$Q(z) = q(0) + \sum_{k=0}^{(N-1)} q(2k+1)(z^{-2k-1} + z^{2k+1}) \tag{8}$$

Thus, the product filter $Q(z)$ is a positive half-band polynomial having $2Z$ zeros at $z = -1$.

The aforementioned non-convex constrained optimization problem will become:

$$\text{minimize} \frac{1}{\pi} \int_{\omega_s}^{\pi} |Q(e^{j\omega})|^2 d\omega \tag{9}$$

subject to

$$q[2m] = \delta(m); \quad m = 0, 1, \dots, (N/2 - 1) \tag{10}$$

$$q(0) + \sum_{n=1}^{N-1} 2(-1)^n q(n) = 0 \tag{11}$$

$$\sum_{k=0}^{N-1} (-1)^k k^{2m} q(k) = 0; \quad m = 0, 1, \dots, Z - 1 \tag{12}$$

$$Q(e^{j\omega}) \geq 0; \quad \omega \in [0, \pi] \tag{13}$$

The above-stated functions are linear on $Q(e^{j\omega})$. Equation (9) is a linear in $q(n)$.

Inequality (13) represents (semi) infinite number of inequality restrictions which are linear. The desired

optimized analysis low-pass filter $C(z)$ can be obtained through the spectral factorization of $Q(z)$, which is the optimal solution of the aforementioned optimization problem (9)–(13).

It is worth noting that the condition (13) represents infinite number of linear constraints, which may lead to the possibility of getting an inexact sub-optimum solution. Therefore, we formulate the design problem as a SDP using positive real and bounded lemmas [17, 24]. This formulation will transform the (semi) infinite linear inequalities into a constraint that can be written into finite linear matrix inequality form. In our study, we have used the Kalman–Yakubovich–Popov (KYP) lemma for the SDP formulation [17], according to which, Eq. (13) is valid if one has a positive-symmetric definite matrix $\mathbf{Q} \in \mathbb{R}^{N \times N}$ such that

$$q(m) = \sum_n [\mathbf{Q}]_{n,n+m}; \quad m = 0, 1, 2, \dots, N - 1 \tag{14}$$

Using (8) and (9), we can express the objective function as a affine function of the autocorrelation sequence $q(n)$ as follows:

$$E_{\text{sp}} = \int_{\omega_s}^{\pi} \left[q(0) + 2 \sum_{k=1}^{(N-1)} q(n) \cos(\omega k) \right] \frac{d\omega}{\pi} = \mathbf{s} \mathbf{q}^T \tag{15}$$

where, \mathbf{s} is a N -length row-vector and given by:

$$\mathbf{s} = \begin{cases} \frac{(\pi - \omega_s)}{\pi}, & \text{for } k = 0 \\ \frac{2 \sin(\frac{\pi}{k} \omega_s)}{k\pi}, & \text{for } 1 \leq k \leq N - 1 \end{cases}$$

and $\mathbf{q} = [q(0), q(1), q(2), \dots, q(N - 1)]$

The objective function in above equation is a linear function of $q(n)$. The orthogonality and regularity constraints can be formulated as finite convex constraints in the variable $q(n)$ in the optimization problem given below

$$\text{minimize } E_{\text{sp}} = \mathbf{s} \mathbf{q}^T \tag{16}$$

$\mathbf{P}_{\geq 0, q[k]}$

subject to (10), (11), (12), (14)

The benefit of using Eq. (16) is that we will not have to tackle the infinite constraints presented by Eq. (13).

As the optimization problem is convex, so for the purpose of obtaining a optimal global solution, we can employ interior point algorithm. To solve the proposed optimization problem, we employ CVX toolbox developed by Grant et al. [22]. The CVX software calls SDPT3 or SeDumi [9, 49]. Next step after finding optimal product filter $Q(z)$ is to obtain the required analysis low-pass filter $C(z)$ via spectral factorization. Spectral factorization gives various choices for selecting optimal filter. We chose the filter (spectral factor), which has minimum phase. Thus, we have obtained optimal orthogonal analysis low-pass filter $C^*(z)$

and other optimal three filters can be derived from $C^*(z)$ [59].

5.3 Design illustrations

In the following section, we have presented two filter design examples.

1. We chose a filter with length fourteen having single vanishing moment and the cutoff frequency was set at $\pi/2$. The minimal stop band energy achieved was 0.0369. The pole-zero plot for the optimal filter is presented in Fig. 5, and the frequency responses are shown in Figs. 6 and 7. Table 2 lists down the filter coefficients. Scaling and wavelet functions, which are generated through iterations of the cascade algorithm [59, 70] are shown in Figs. 8 and 9, respectively.
2. Next, we design filter of length eighteen with five vanishing moments. For this filter, the cutoff frequency is $\pi/2$. The stop band energy for the optimal filter is $E_{sp} = 0.033$. Figure 10 depicts pattern of poles and zeros of the derived optimal filter. The frequency responses are shown in Figs. 11 and 12. The coefficients for this filter are provided in Table 2. Scaling and wavelet functions are shown in Figs. 13 and 14, respectively.

We have used above optimal filters in this study to obtain SBs of ECG signals. Figure 3 shows the sample ECG signals. The six decomposed SBs for the sample shockable and non-shockable signals are shown in Figs. 15 and 16. The SB are obtained using optimal filter of design example-1.

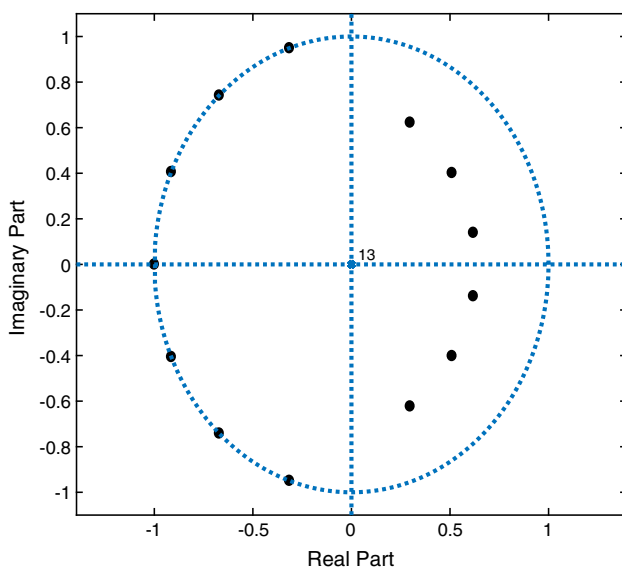


Fig. 5 Pole-zero plot for example 1

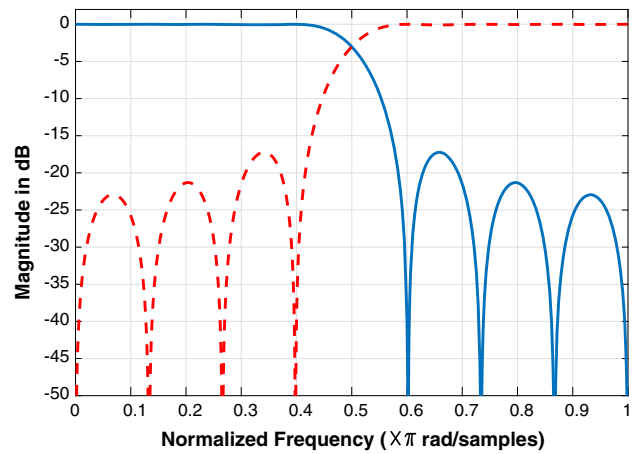


Fig. 6 Frequency response of designed filter in example 1. Dashed line represents HPF and solid line represents LPF

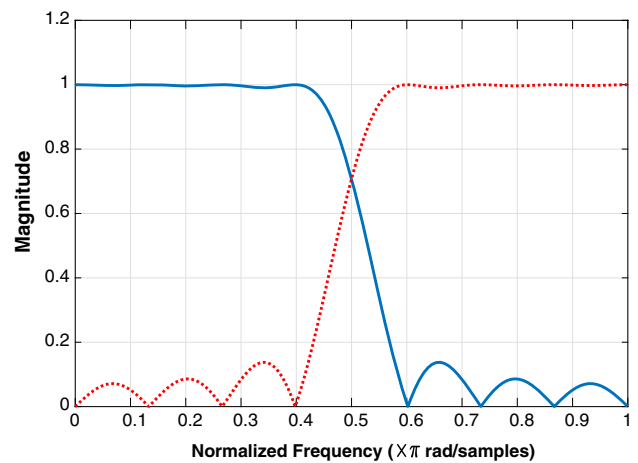


Fig. 7 Frequency response of designed filter in example 1. Dashed line represents HPF and solid line represents LPF

6 Features extraction and statistical analysis

Having obtained six SBs of each ECG epoch, we extracted fuzzy entropy (FE) and Renyi entropy (RenE) of each SB. To evaluate the discrimination ability of an individual feature, we have employed t test to rank all the extracted features. We have also used Kruskal–Wallis test (KWT) to calculate the p values corresponding to each feature.

6.1 Fuzzy entropy (FE)

The characteristic of signal used for determining the regularity of a time series is fuzzy entropy [51]. It is applied to get precise output from imprecise inputs. Fuzzy sets [69] are applied to determine the FE of a signal and can be studied further in [14]. Acharya et al. [3] presented use of entropy for the detection of epilepsy. In our work, FE of

Table 2 Optimal filter coefficients for the designed filters

Index	Example-1	Example-2
0	3.5882×10^{-1}	1.9116×10^{-1}
1	6.9973×10^{-1}	6.0827×10^{-1}
2	5.2772×10^{-1}	6.5990×10^{-1}
3	3.5590×10^{-3}	1.9376×10^{-1}
4	-2.4295×10^{-1}	-2.0737×10^{-1}
5	-4.3233×10^{-2}	-1.6979×10^{-1}
6	1.4473×10^{-1}	1.1036×10^{-1}
7	3.6880×10^{-2}	1.1542×10^{-1}
8	-9.9208×10^{-2}	-6.5557×10^{-2}
9	-2.2908×10^{-2}	-7.9149×10^{-2}
10	7.4260×10^{-2}	3.7763×10^{-2}
11	4.2128×10^{-3}	7.1062×10^{-2}
12	-5.6274×10^{-2}	-5.0459×10^{-2}
13	2.8857×10^{-2}	-3.5978×10^{-2}
14	–	4.4841×10^{-2}
15	–	-7.5361×10^{-4}
16	–	-1.3544×10^{-2}
17	–	4.2567×10^{-3}

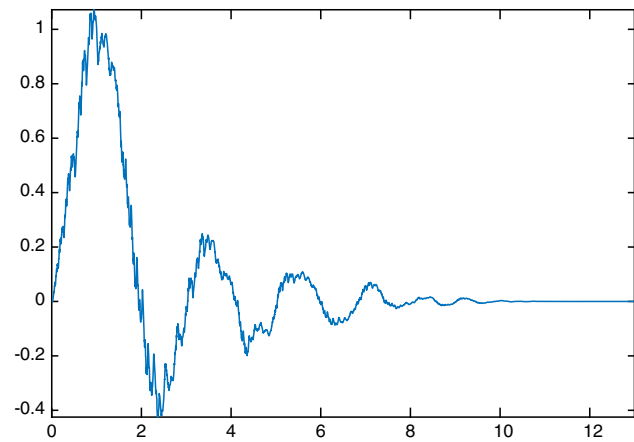


Fig. 8 Scaling plot for example 1. X and Y axes represent time and amplitude, respectively

wavelet series of ECG signals were calculated and then was averaged.

6.2 Renyi entropy (RE)

It is defined as the negative logarithm of summation of energy [41]. RE is given by:

$$\text{RenE}_i = -\log \sum |p(n)|^2$$

where $p(n)$ is the signal sequence.

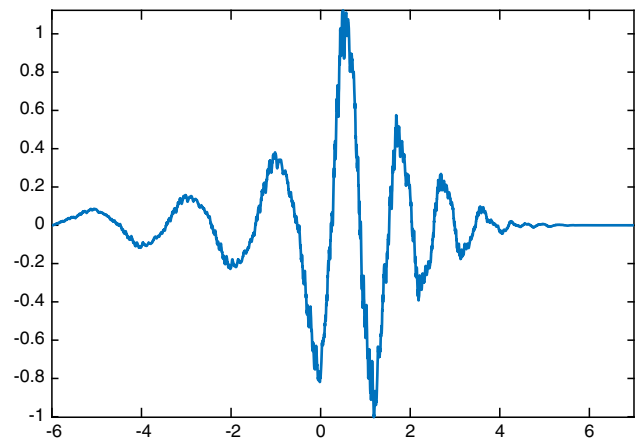


Fig. 9 Wavelet plot for example 1. X and Y axes represent time and amplitude respectively

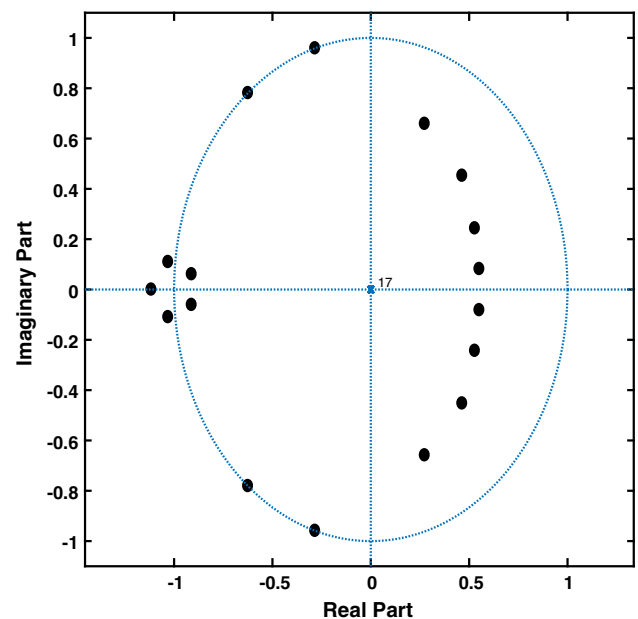


Fig. 10 Pole-zero plot for example 2

Thus, we have commuted total 12 features (6 features each for FE and RE corresponding to each of six SBs). The computed features have been ranked using t test based on the their t values.

7 Results

The results are presented in this section. We have tested many supervised machine learning classifiers such as K-nearest neighbors, linear discriminant, quadratic discriminant, complex tree and SVM to separate features corresponding to SAR and NSAR. Table 3 gives classification accuracy obtained using various classifiers. It is to be noted that first, we tested these classifiers using their

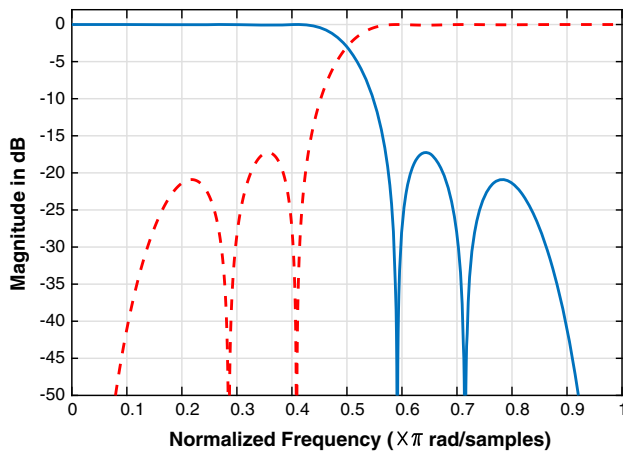


Fig. 11 Frequency response of designed filter in example 2. Dashed line represents HPF and solid line represents LPF

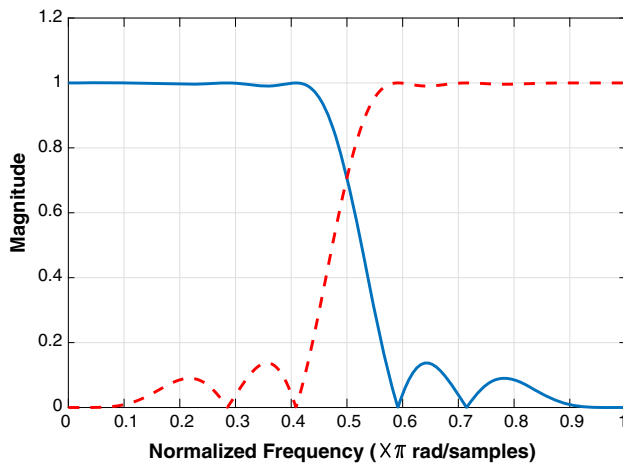


Fig. 12 Frequency response of designed filter in example 2. Dashed line represents HPF and solid line represents LPF

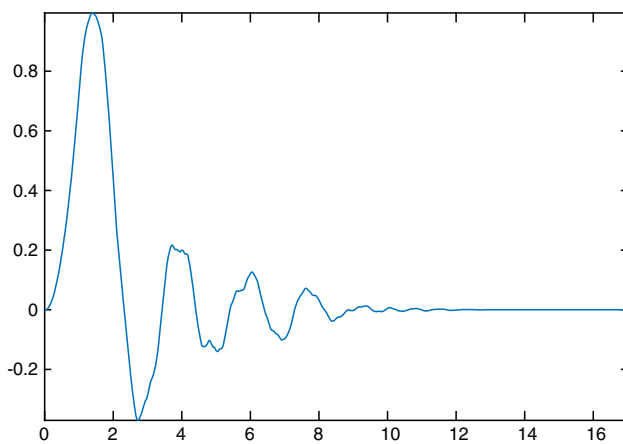


Fig. 13 Scaling plot for example 2. X and Y axes represent time and amplitude respectively

default values in Matlab Release-12. When default parameters are chosen, we found the highest performance

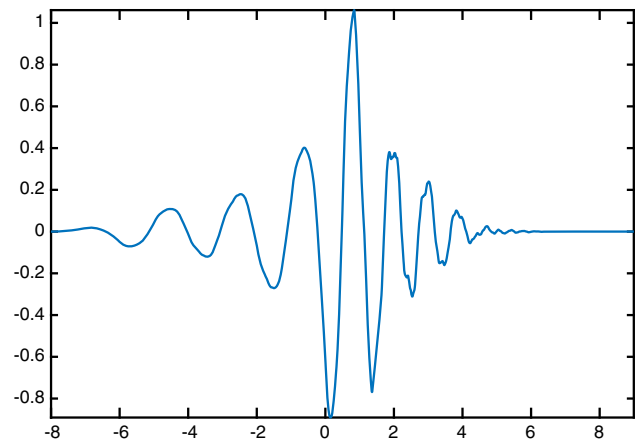


Fig. 14 Wavelet plot for example 2. X and Y axes represent time and amplitude respectively

with Gaussian SVM for kernel scale $\sigma = 1$ and box constraint $BC = 1$. Then, we tuned the parameters of Gaussian SVM to obtain the optimal classification accuracy using sequential minimal optimization routine. We have varied kernel scale in the range $[.1 \ 100]$ and box constraint in range $[1, \ 100]$. We obtained the best results with Gaussian SVM with $\sigma = 1.2, BC = 8$. In order to provide a fair comparison, we have tested the same model using standard db-6 wavelet-based features employing the same method. From Table 3, it is clear that our optimal wavelet filter-based features perform better than db-6 wavelet-based features. We can see from the table that the highest accuracy achievable through db-6 wavelet-based features is 95.2%, whereas our optimal wavelet filter bank features attain maximum accuracy of 97.8%. During classification, we classified the features using different kernels of SVM. We used linear, quadratic, cubic and Gaussian kernels, and achieved the respective Accs of 95.2%, 97.2%, 97.8% and 97.7% respectively. Thus, the SVM classifier with cubic kernel function surpassed the performance of SVM classifier with other Kernel function. Table 4 shows the confusion matrix corresponding to the cubic SVM that obtain the highest classification accuracy. In the table, TP, TN, FP, FN and PPV [5] denote true positive, true negative, false positive, false negative and positive predictive value, respectively. It can be seen from the confusion matrix that the highest accuracy of 97.8%, the sensitivity of 93.42% and specificity of 98.35% were obtained when classified using a combination of RE and FE features. Taking RE and FE features individually during the classification task also yielded good performance with an accuracy of 97.3% and 97.5%, respectively. Figures 17, 18 and 19 show the ROC plots for both the features(RE and FE) when taken separately as well as jointly. From figures, it is clear that the proposed method achieved area under ROC (AUC) of 0.99, which is very close the perfect value 1. We have also

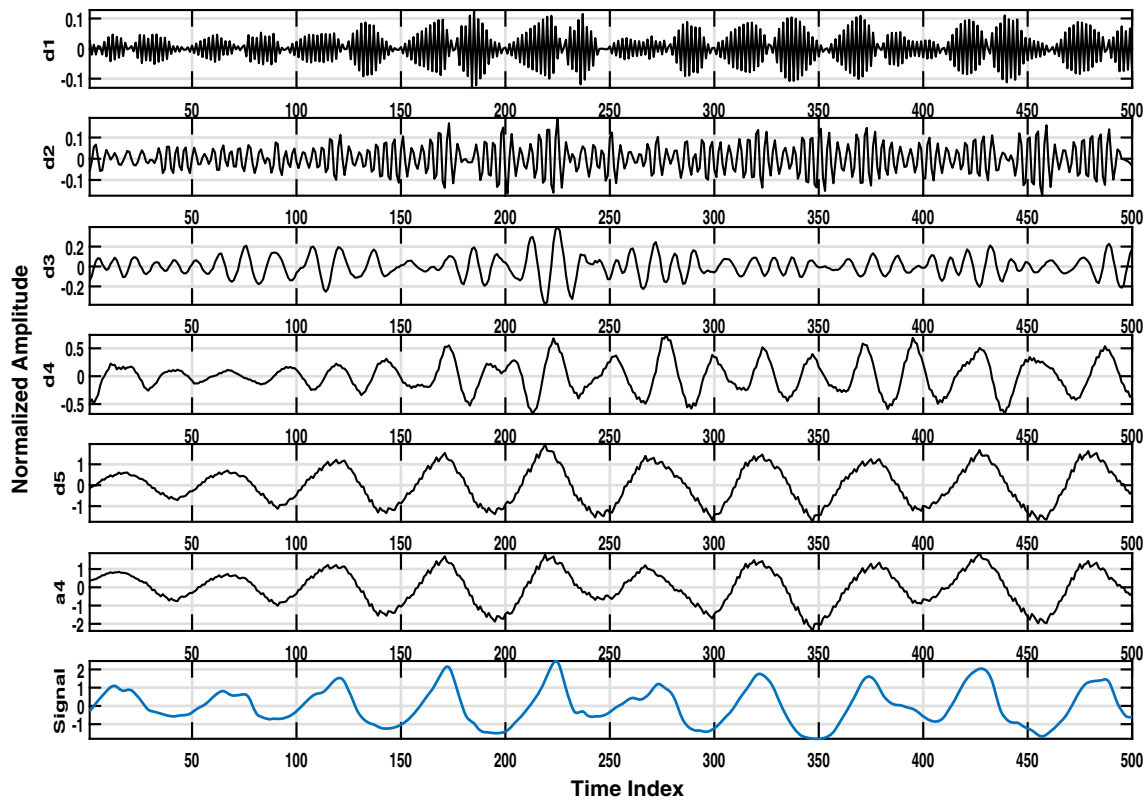


Fig. 15 Decomposed subbands for shockable sample, d1–d5 represents the five detailed subbands, a4 represents the approximate subband

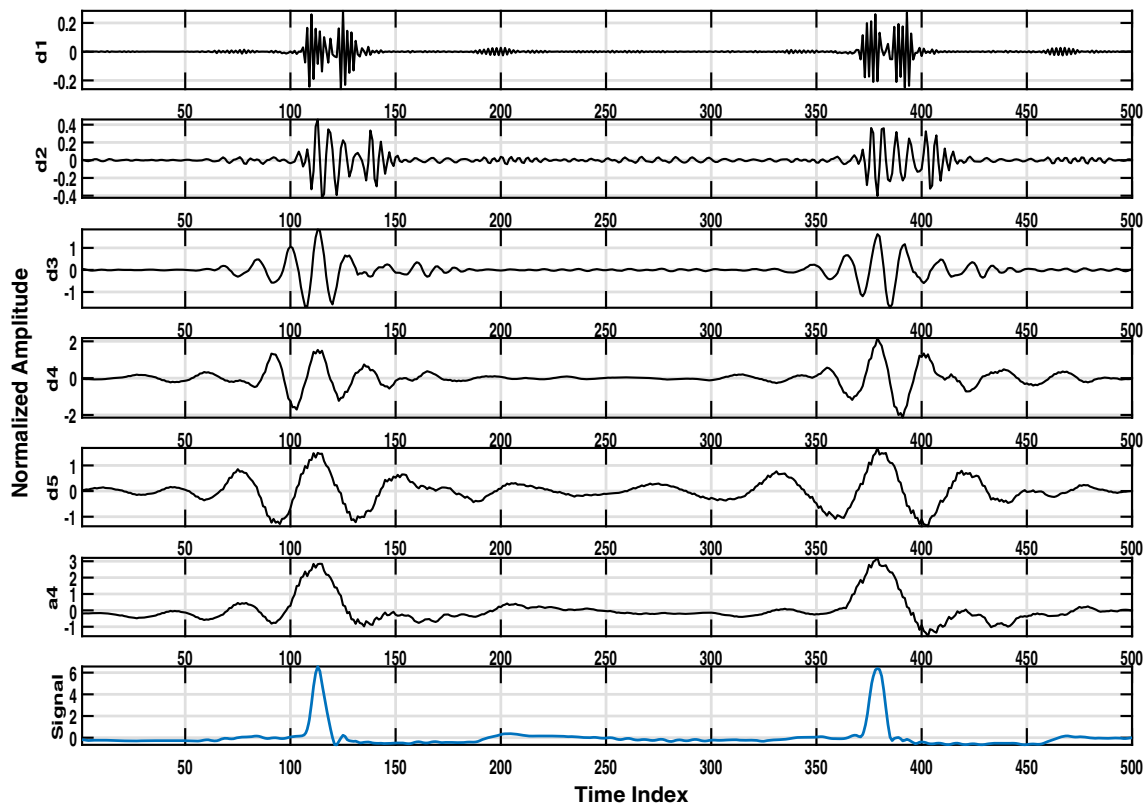


Fig. 16 Decomposed subbands for non-shockable sample, d1–d5 represents the five detailed subbands, a4 represents the approximate subband

Table 3 Comparison of designed optimal wavelet-based features and db-6 wavelet-based features using different classifier

Classifier	ACC% using optimal OWFB-based feature	ACC% using db-6 wavelet-based features
Complex tree	97	95.1
Linear discriminant	91.2	86.6
Quadratic discriminant	90.9	81.1
Logistic regression	94.7	94.1
<i>K</i> nearest neighbors	97.6	94.7
SVM	97.8	95.2

Table 4 Overall classification performance across ten folds

Feature	TP	TN	FP	FN	Acc. (%)	Sen. (%)	Spec. (%)	PPV (%)
RE	47,767	4846	1155	328	97.3	93.66	97.64	99.32
FE	47,794	4932	1069	301	97.5	94.25	97.81	99.37
FE+RE	47,729	5200	801	366	97.8	93.42	98.35	99.24

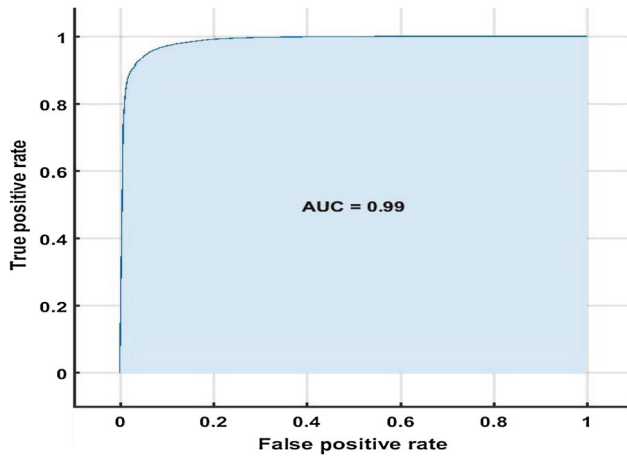


Fig. 17 ROC for FE alone

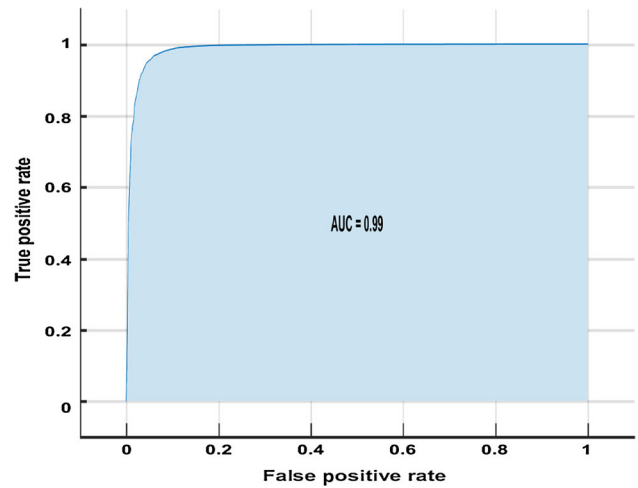


Fig. 19 ROC for FE and RE features taken together

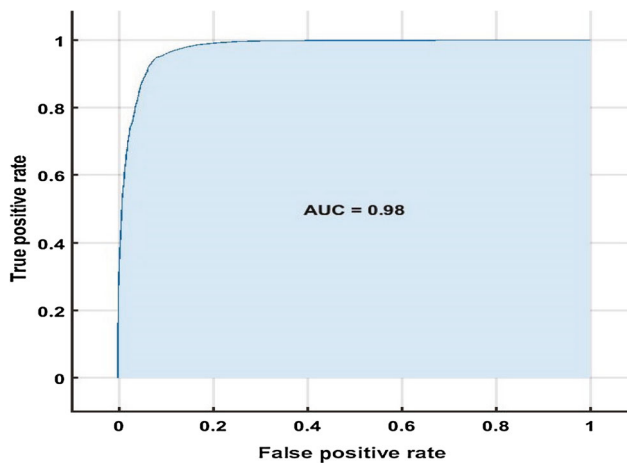


Fig. 18 ROC for RE alone

Table 5 *p* values of the extracted entropy features

Subband	FE	RE
SB-1	0	0
SB-2	0	0
SB-3	1.6881×10^{-05}	0
SB-4	0	0
SB-5	0	0.0129
SB-6	0.0038	3.5353×10^{-05}

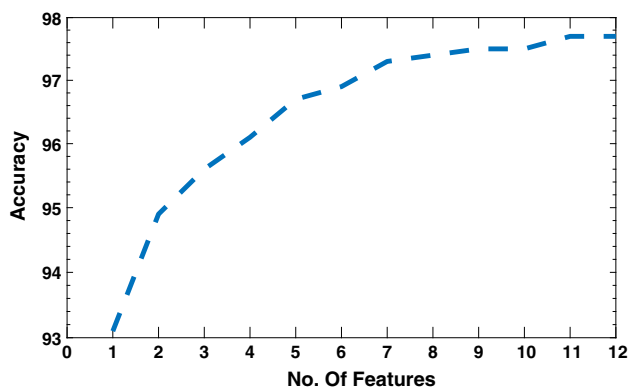
calculated the *F1*-score, which is considered to be a better classification performance indicator than accuracy and AUC in many cases. Interestingly, our method has attained *F1*-score of 0.99 which is close to the perfect value of 1. Thus, the classification performance of the proposed method is represented in terms of accuracy, AUC and *F1*-

Table 6 Statistical results (mean \pm standard deviation) and ranking of FE

SBs	FE		Rank
	NSER	SR	
SB-1	0.0463 \pm 0.0135	0.0637 \pm 0.0273	5
SB-2	0.0034 \pm 0.0282	− 0.0705 \pm 0.0326	1
SB-3	0.1226 \pm 0.0586	0.1193 \pm 0.0594	11
SB-4	0.1762 \pm 0.05326	0.2208 \pm 0.0526	4
SB-5	0.1387 \pm 0.0360	0.1272 \pm 0.0454	9
SB-6	0.1023 \pm 0.0205	0.1013 \pm 0.0376	12

Table 7 Statistical results (mean \pm standard deviation) and ranking of RE

SBs	RE		Rank
	NSER	SR	
SB-1	− 10.9671 \pm 0.5800	− 11.3664 \pm 0.7235	6
SB-2	− 5.0837 \pm 0.4273	− 5.4782 \pm 0.7412	7
SB-3	− 6.5807 \pm 0.7690	− 6.3507 \pm 0.6304	8
SB-4	8.5641 \pm 0.9956	− 7.1881 \pm 0.9524	2
SB-5	− 9.7121 \pm 0.7795	− 8.5527 \pm 0.9786	3
SB-6	− 10.1636 \pm 0.5610	− 10.3502 \pm 1.0721	10

**Fig. 20** Plot of accuracy versus number of features

score. Further, the p values are mentioned in Table 5. From Table 5, we can see that p values of all the features are less than the significant level 0.01. Tables 6 and 7 give the mean, standard deviation and ranking of FE and RE features corresponding to each of the six SBs to have an estimation of classification capability of each feature individually. We have plotted accuracy with respect to the number of ranked features in Fig. 20.

8 Discussion

- From Table 4, it is clear that fuzzy entropy wavelet-based features performed better than RE wavelet-based in terms of Acc., Sen., Spec. and PPV. From Fig. 19, it is also evident that FE wavelet-based features discriminate NSAR and SAR better than RE wavelet-based features, as the AUC of FE wavelet-based features is higher than the RE wavelet-based features. Combining both features in the classification process improved the classification performance.
- From Table 8, we can see that various automated systems have used different window lengths (WL) (10 s, 8 s, 6 s, 5 s and 2 s) for processing ECG epochs. For the implementation of fast real-time system, a short window length is desirable because the smaller the WL, the faster would be the system. It is clear that our proposed system has used the shortest WL. It is to be noted that in the recent work by Acharya et al. [2], authors have also used the shortest window length of 2 s. However, the classification performance of the proposed model by us is better than their model. It is worth noting that despite the proposed model by us uses the shortest WL of 2 s, it outperformed the other models which used longer WL of duration > 2 s. Thus the proposed model is not only accurate but also faster than other models listed in the Table 8.
- In Table 5, we can notice the p values of all 12 features are less than the chosen significant level of .01; hence, all features are statistically significant.
- From Table 6, we can observe that the mean values of FE of SB-2, SB-3, SB-5 and SB-6 for NSAR are more than the corresponding SAR. Similarly, the mean values FE of SB-1 and SB-4 for SAR are more than the corresponding NSAR. And the mean values for RE of SB-1, SB-2 and SB-6 for NSAR are more than the corresponding SAR. Also the mean values RE of SB-3, SB-4 and SB-5 for SAR are more than the corresponding NSAR.
- From Table 6, we can see that FE corresponding to the SB-2 is the topmost ranked feature, while the SB-6 is the least ranked feature. The ranking was done using student's t test.
- We have performed all the experiments using Matlab software with a computer equipped with an Intel's Xeon 3.5 GHz processor and 16 GB RAM. The model completed whole training process in 39.53 s and the prediction speed of the classifier was found to be 23,000 obs/s.
- We studied the reliability of the optimal wavelet-based entropy features in order to advise an appropriate shock, which decides the type of arrhythmia (shockable or

Table 8 Comparison with previous works using the same database

Reference	Methodology/WL	Performance
Jekova [25]	Five previously proposed methods were reviewed/10 s	Sen: 94% Spec: 91%
Jekova and Krasteva [27]	Band-pass filtering/10 s	Sen: 94.45% Spec: 95.9%
Amann et al. [7]	Twelve different time-delay methods/8 s	Sen: 79% Spec: 98.5% Acc: 96.2%
Jekova [26]	Discriminant analysis/10 s	Sen: 94.1% Spec: 93.8%
Fokkenrood et al. [19]	Amplitude distribution analysis/6 s	Sen: 97% Spec: 98% Acc: 98%
Alonso-Atienza et al. [6]	Morphological, spectral and complexity features of ECG Support vector machine/8 s	Sen: 92% Spec: 97%
Li et al. [32]	VF-filter leakage measure Auxiliary counts Support vector machine/5 s	Sen: 96.2% Spec: 96.2% Acc: 96.3%
Tripathy et al. [62]	Variational mode decomposition Renyi entropy and permutation entropy Random forest classifier/8 s	Sen: 96.54% Spec: 97.97 % Acc: 97.23%
Acharya et al. [2]	Convolution neural Network (CNN)/2 s	Sen: 95.32% Spec: 91.04% Acc: 93.18%
In the presented work	Features extracted FE/2s RE/2 s Classification method SVM	Sen: 93.42% Spe: 98.35% Acc: 97.8% F1-score: 0.99

non-shockable). The efficacy of SAR detection system was evaluated by employing it in an automated external defibrillator system.

- One of the advantages of the proposed system is that, it does not require pre-processing on ECG signals unlike the other methods [6, 7, 19, 26] which employ complex pre-processing. Also, we chose ECG epochs of 2 s without any preselection and our algorithm does not need to detect R-peaks.
- In this study, we have used only 12 features to characterize NSARs and SARs epochs of duration 2 s, whereas Alonso-Atienza et al. [6] extracted 13 features with epochs of length 8 s. Despite this, our system classified NASRs and SARs better than the system by Alonso-Atienza et al. [6]. Though Tripathy et al. [62] computed only 9 features, they used a window length of 8 s to get their best results. Moreover, they used VMD decomposition to obtain modes of ECG epochs. We have used optimal orthogonal wavelet decomposition to obtain wavelet SBs. The VMD-based mode decomposition is computationally more expensive than wavelet-

based decomposition. Thus our system is more accurate, computationally less expensive and faster than the recent system by Tripathy et al. [62]. Further, it is to be noted that Tripathy et al. [62] also computed RE features for their VMD-based modes. However, the intrinsic mode-based RE features could attain AUC of 0.644, whereas our wavelet-based RE features attain AUC of 0.98. Li et al. [32] also used 9 features using various window lengths, and obtained best results using 10 s WL as shown in Table 8. Using 2 s WL, their model attained Acc of 95.2%, Sen of 95.1% and Spec of 95.1%. Thus, our model distinguishes NSARs and SARs better than Li et al. [32]. Recently, Acharya et al. [2] have introduced CNN-based system which does not require the extraction of features using epochs of 2 s; however, the proposed system by us performed significantly better than their system in terms of Acc, Sen and Spec. It is to be noted that in CNN-based methods, one need not to extract the features and takes a long time to develop the model. Our system takes only 39.52 s for the whole training process. Hence, the proposed system

can be considered more accurate and faster than the system by Acharya et al. [2].

- The assessment of a model using only Acc may be sometimes misleading. So, *F1*-score and AUC are considered to be better measures to valuate the performance of an algorithm. It is to be noted that our model not only performed well in terms of Acc, Sen and Spec but it also yielded high *F1*-score of 0.99 and AUC of 0.99.
- The VF and VT with heart rate > 180 beats/min are considered as very serious cardiac disorders that can cause severe brain injury as well as death if the patient is not given defibrillation shock immediately using AED. Both VF and VT have high heart rates; hence, fast and accurate detection algorithm is essential for the AED system. Since the model achieved the specificity of 98.35% and *F1*-score of 0.99, which is the highest among all existing state-of-the-art methods, the proposed model reduces the chances of false defibrillations. Also, our proposed algorithm presents high classification performance in terms of *F1*-score and AUC. Hence, it can be integrated in AED for emergency resuscitation of SCD and to save lives. The accurate model reduces the possibility of the damage caused to the heart due to the misclassification of either NSAR or SAR.
- In the literature, to analyze physiological signals, including ECG wavelet-based methods have been used [47]. However, most of these methods have employed traditional standard Daubechies wavelet (db)-based features [15]. The db wavelet filters, however, are not optimal wavelet in any sense. In this study, we have used a new class of optimal orthogonal wavelet filter banks for analyzing ECG signals; this is the novelty of the proposed study. Further, for SAR detection, state-of-the-art methods employ various signal processing; machine-learning- and deep-learning-based methods (refer Table 8). However, wavelet-based features have yet not been explored for SAR detection to the best of our knowledge. We are the one those have used very first-time optimal wavelet-based features for the detection of the shockable ventricular arrhythmia. Furthermore, most of the existing methods for SAR detections employ ECG epochs of the duration of either 10 s or 8 s; in the proposed study by us, we have used epochs of duration 2 s only despite it, our system has surpassed others in terms of classification performance.

9 Conclusion

We have evaluated the performance of optimal wavelet-based entropy features in the proposed method for automated discrimination of NSAR and SAR of ECG. The performance of

our developed system surpasses existing state-of-the-art detection systems in terms of classification performance, window length and speed. In the presented work, we employed an optimal two-channel frequency selective orthogonal filter to obtain sub-bands of ECG signals. The proposed system exhibits high potential in detecting shockable rhythms using optimal wavelet filter bank-based entropy features. FE and RE features of the data were calculated and were fed into the SVM classifier. We tested our method on ECG signals consisting of shockable and non-shockable heartbeats. The overall accuracy of 97.8% sensitivity and specificity of 93.42% and 98.35% were achieved, respectively. Hence, the proposed automated system establishes the suitability of wavelet-based features in the diagnosis of shockable ventricular arrhythmia and may help the doctors in deciding if a shock treatment need to be delivered urgently. Further, the proposed system employs short-duration ECG epochs of 2 s, which reduces the computational load of extricating features and makes the system fast that can also be considered as a candidate for real-time detection of SAR. Moreover, in this study, we have used three databases comprising total 54,096 ECG segments which make the database the largest freely available data set used for SAR. The limitation of the proposed study is that we have used a limited number of subjects in NSAR and SAR classes. In the future, we intend to use more subjects in both classes. The performance of our method may be examined in the presence of severe noise as a future study. Recently, Acharya et al. [2] have employed CNN-based deep learning (DL) method to detect ECG-SAR. It would be interesting to evaluate the performance of some new DL techniques including LSTM [1, 4, 5, 38–40, 65–68]. It would be interesting to use the proposed wavelet as a wavelet sequence in a deep neural network in the detection of ECG-SAR. The new optimal filter bank-based features may be examined in the automated detection of some other cardiac disorders. Further, in this study, we have used only two entropy-based features, using the same optimal filter bank. In the future, we can extract some other nonlinear features such as Hurt exponent, Lyapunov exponent, fractal and correlation dimensions to improve the performance of these new wavelet-based features in SAR detection. Recently, Sharma et al. [43, 47, 60] designed novel time-frequency optimized orthogonal and biorthogonal wavelet filter banks. We can explore to observe the performance of the features obtained using these new filter banks for this study.

Compliance with ethical standards

Conflict of interest None of the authors have any conflict of interest. We also would like to declare that we do not have any competing interests.

References

- Acharya UR, Fujita H, Oh SL, Hagiwara Y, Tan JH, Adam M (2017) Application of deep convolutional neural network for automated detection of myocardial infarction using ECG signals. *Inf Sci* 415:190–198
- Acharya UR, Fujita H, Oh SL, Raghavendra U, Tan JH, Adam M, Gertych A, Hagiwara Y (2018) Automated identification of shockable and non-shockable life-threatening ventricular arrhythmias using convolutional neural network. *Future Gener Comput Syst* 79:952–959
- Acharya UR, Molinari F, Sree SV, Chattopadhyay S, Ng KH, Suri JS (2012) Automated diagnosis of epileptic eeg using entropies. *Biomed Signal Process Control* 7(4):401–408
- Acharya UR, Oh SL, Hagiwara Y, Tan JH, Adam M, Gertych A, San Tan R (2017) A deep convolutional neural network model to classify heartbeats. *Comput Biol Med* 89:389–396
- Acharya UR, Oh SL, Hagiwara Y, Tan JH, Adeli H (2017) Deep convolutional neural network for the automated detection and diagnosis of seizure using EEG signals. *Comput Biol Med* 100:270–278
- Alonso-Atienza F, Morgado E, Fernandez-Martinez L, García-Alberola A, Rojo-Alvarez JL (2014) Detection of life-threatening arrhythmias using feature selection and support vector machines. *IEEE Trans Biom Eng* 61(3):832–840
- Amann A, Tratnig R, Unterkofler K (2007) Detecting ventricular fibrillation by time-delay methods. *IEEE Trans Biomed Eng* 54(1):174–177
- Barro S, Ruiz R, Cabello D, Mira J (1989) Algorithmic sequential decision-making in the frequency domain for life threatening ventricular arrhythmias and imitative artefacts: a diagnostic system. *J Biomed Eng* 11(4):320–328
- Bhati D, Sharma M, Pachori RB, Gadre VM (2017) Time-frequency localized three-band biorthogonal wavelet filter bank using semidefinite relaxation and nonlinear least squares with epileptic seizure EEG signal classification. *Digit Signal Process* 62:259–273
- Bhattacharyya A, Sharma M, Pachori RB, Sircar P, Acharya UR (2018) A novel approach for automated detection of focal EEG signals using empirical wavelet transform. *Neural Comput Appl* 29(8):47–57
- Caglar H, Liu Y, Akansu AN (1991) Statistically optimized PR-QMF design. In: *Proceedings of SPIE*, vol 1605, pp 86–94
- Chandrasekhar E, Dimri V, Gadre VM (2013) *Wavelets and fractals in earth system sciences*. Taylor & Francis, London
- Chen S, Thakor N, Mower M (1987) Ventricular fibrillation detection by a regression test on the autocorrelation function. *Med Biol Eng Comput* 25(3):241–249
- Chen W, Wang Z, Xie H, Yu W (2007) Characterization of surface emg signal based on fuzzy entropy. *IEEE Trans Neural Syst Rehabil Eng* 15(2):266–272
- Daubechies I (1992) *Ten lectures on wavelets*, vol 61. SIAM, Philadelphia
- Dumitrescu B, Tabus I, Stoica P (2001) On the parameterization of positive real sequences and ma parameter estimation. *IEEE Trans Signal Process* 49(11):2630–2639. <https://doi.org/10.1109/78.960409>
- Dumitrescu B, Tabus I, Stoica P (2001) On the parameterization of positive real sequences and MA parameter estimation. *IEEE Trans Signal Process* 49(11):2630–2639
- Fan A, Han P, Liu B (2012) Shockable rhythm detection algorithms for electrocardiograph rhythm in automated defibrillators. *AASRI Proc* 1:21–26
- Fokkenrood S, Leijdekkers P, Gay V (2007) Ventricular tachycardia/fibrillation detection algorithm for 24/7 personal wireless heart monitoring. In: *International conference on smart homes and health telematics*, pp 110–120. Springer
- Gaziano TA (2005) Cardiovascular disease in the developing world and its cost-effective management. *Circulation* 112(23):3547–3553
- Goldberger AL, Amaral LA, Glass L, Hausdorff JM, Ivanov PC, Mark RG, Mietus JE, Moody GB, Peng CK, Stanley HE (2000) *Physiobank, physiotoolkit, and physionet*. *Circulation* 101(23):e215–e220
- Grant M, Boyd S (2012) CVX: Matlab software for disciplined convex programming, version 2.0 beta. <http://cvxr.com/cvx>. Accessed 12 Jan 2015
- Greenwald SD (1986) *The development and analysis of a ventricular fibrillation detector*. PhD thesis, Massachusetts Institute of Technology
- Hitz L, Anderson B (1969) Discrete positive-real functions and their application to system stability. In: *Proceedings of the Institution of Electrical Engineers*, vol 116, pp 153–155. IET
- Jekova I (2000) Comparison of five algorithms for the detection of ventricular fibrillation from the surface ECG. *Physiol Meas* 21(4):429
- Jekova I (2007) Shock advisory tool: detection of life-threatening cardiac arrhythmias and shock success prediction by means of a common parameter set. *Biomed Signal Process Control* 2(1):25–33
- Jekova I, Krasteva V (2004) Real time detection of ventricular fibrillation and tachycardia. *Physiol Meas* 25(5):1167
- Karmakar A, Kumar A, Patney R (2007) Design of an optimal two-channel orthogonal filterbank using semidefinite programming. *IEEE Signal Process Lett* 14(10):692–694
- Kuo S (1978) Computer detection of ventricular fibrillation. In: *Proceedings of computers in cardiology*. IEEE Computer Society, pp 347–349
- Kutsogiannis DJ, Bagshaw SM, Laing B, Brindley PG (2011) Predictors of survival after cardiac or respiratory arrest in critical care units. *Can Med Assoc J* 183(14):1589–1595. <https://doi.org/10.1503/cmaj.100034>
- Laslett LJ, Alagona P, Clark BA, Drozda JP, Saldivar F, Wilson SR, Poe C, Hart M (2012) The worldwide environment of cardiovascular disease: prevalence, diagnosis, therapy, and policy issues: a report from the american college of cardiology. *J Am Coll Cardiol* 60(25):S1–S49
- Li Q, Rajagopalan C, Clifford GD (2014) Ventricular fibrillation and tachycardia classification using a machine learning approach. *IEEE Trans Biomed Eng* 61(6):1607–1613
- Moody GB, Mark RG (2001) The impact of the MIT-BIH arrhythmia database. *IEEE Eng Med Biol Mag* 20(3):45–50
- Moulin P, Anitescu M, Kortanek KO, Potra FA (1997) The role of linear semi-infinite programming in signal-adapted QMF bank design. *IEEE Trans Signal Process* 45(9):2160–2174
- Muthuvel A, Makur A (2000) Design of two-channel linear-phase FIR PR filter banks with even length filters using convolution matrices. *IEEE Trans Circuits Syst II Analog Digit Signal Process* 47(12):1413–1418
- Nolle F, Badura F, Catlett J, Bowser R, Sketch M (1986) CREI-GARD, a new concept in computerized arrhythmia monitoring systems. *Comput Cardiol* 13:515–518
- Padmavati S (1962) Epidemiology of cardiovascular disease in India: II. Ischemic heart disease. *Circulation* 25(4):711–717
- Plawiak P (2018) Novel genetic ensembles of classifiers applied to myocardium dysfunction recognition based on ECG signals. *Swarm Evol Comput* 39:192–208. <https://doi.org/10.1016/j.swevo.2017.10.002>
- Plawiak P (2018) Novel methodology of cardiac health recognition based on ECG signals and evolutionary-neural system.

- Expert Syst with Appl 92:334–349. <https://doi.org/10.1016/j.eswa.2017.09.022>
40. Plawiak P, Acharya UR (2018) Novel deep genetic ensemble of classifiers for arrhythmia detection using ECG signals. *Neural Comput Appl*. <https://doi.org/10.1007/s00521-018-03980-2>
 41. Renner R, Wolf S (2004) Smooth rényi entropy and applications. In: ISIT 2004. Proceedings. International symposium on information theory, 2004, p 233. IEEE
 42. Roth GA, Johnson C, Abajobir A, Abd-Allah F, Abera SF, Abyu G, Ahmed M, Aksut B (2017) Global, regional, and national burden of cardiovascular diseases for 10 causes, 1990 to 2015. *J Am Coll Cardiol* 70:1–25
 43. Sharma M, Acharya UR (2018) Analysis of knee-joint vibroarthrographic signals using bandwidth-duration localized three-channel filter bank. *Comput Electr Eng* 72:191–202
 44. Sharma M, Pachori RB, Acharya UR (2017) A new approach to characterize epileptic seizures using analytic time-frequency flexible wavelet transform and fractal dimension. *Pattern Recogn Lett* 94:172–179. <https://doi.org/10.1016/j.patrec.2017.03.023>
 45. Sharma M, Achuth P, Deb D, Puthankattil SD, Acharya UR (2018) An automated diagnosis of depression using three-channel bandwidth-duration localized wavelet filter bank with EEG signals. *Cogn Syst Res* 52:508–520
 46. Sharma M, Achuth PV, Pachori RB, Gadre VM (2017) A parametrization technique to design joint time-frequency optimized discrete-time biorthogonal wavelet bases. *Signal Process* 135:107–120
 47. Sharma M, Agarwal S, Acharya UR (2018) Application of an optimal class of antisymmetric wavelet filter banks for obstructive sleep apnea diagnosis using ECG signals. *Comput Biol Med* 100:100–113. <https://doi.org/10.1016/j.combiomed.2018.06.011>
 48. Sharma M, Bhati D, Pillai S, Pachori RB, Gadre VM (2016) Design of time-frequency localized filter banks: transforming non-convex problem into convex via semidefinite relaxation technique. *Circuits Syst Signal Process* 35(10):3716–3733
 49. Sharma M, Bhurane AA, Acharya UR (2018) MMSFL-OWFB: a novel class of orthogonal wavelet filters for epileptic seizure detection. *Knowl Based Syst* 160:265–277. <https://doi.org/10.1016/j.knosys.2018.07.019>
 50. Sharma M, Deb D, Acharya UR (2017) A novel three-band orthogonal wavelet filter bank method for an automated identification of alcoholic EEG signals. *Appl Intell* 48:1368
 51. Sharma M, Dhere A, Pachori RB, Acharya UR (2017) An automatic detection of focal EEG signals using new class of time-frequency localized orthogonal wavelet filter banks. *Knowl Based Syst* 118:217–227
 52. Sharma M, Dhere A, Pachori RB, Gadre VM (2017) Optimal duration-bandwidth localized antisymmetric biorthogonal wavelet filters. *Signal Process* 134:87–99
 53. Sharma M, Gadre VM, Porwal S (2015) An eigenfilter-based approach to the design of time-frequency localization optimized two-channel linear phase biorthogonal filter banks. *Circuits Syst Signal Process* 34(3):931–959
 54. Sharma M, Goyal D, Achuth P, Acharya UR (2018) An accurate sleep stages classification system using a new class of optimally time-frequency localized three-band wavelet filter bank. *Comput Biol Med* 98:58–75. <https://doi.org/10.1016/j.combiomed.2018.04.025>
 55. Sharma M, Sharma P, Pachori RB, Acharya UR (2018) Dual-tree complex wavelet transform-based features for automated alcoholism identification. *Int J Fuzzy Syst* 20(5):1297–1308
 56. Sharma M, Sharma P, Pachori RB, Gadre VM (2019) Double density dual-tree complex wavelet transform based features for automated screening of knee-joint vibroarthrographic signals. In: 2019 international conference on machine intelligence and signal analysis, advances in intelligent systems and computing, vol 748. Springer, Singapore, pp 279–290. https://doi.org/10.1007/978-981-13-0923-6_24
 57. Sharma M, Kolte R, Patwardhan P, Gadre V (2010) Time-frequency localization optimized biorthogonal wavelets. In: International conference on signal processing and communications (SPCOM), pp 1–5
 58. Sharma M, Singh T, Bhati D, Gadre V (2014) Design of two-channel linear phase biorthogonal wavelet filter banks via convex optimization. In: 2014 international conference on signal processing and communications (SPCOM), pp 1–6. <https://doi.org/10.1109/SPCOM.2014.6983931>
 59. Sharma M, Vanmali AV, Gadre VM (2013) Construction of wavelets: principles and practices in wavelets and fractals in earth system sciences. CRC Press, Taylor and Francis Group, Boca Raton
 60. Sharma M, Tan RS, Acharya UR (2018) A novel automated diagnostic system for classification of myocardial infarction ECG signals using an optimal biorthogonal filter bank. *Comput Biol Med*. <https://doi.org/10.1016/j.combiomed.2018.07.005>
 61. Thakor NV, Zhu YS, Pan KY (1990) Ventricular tachycardia and fibrillation detection by a sequential hypothesis testing algorithm. *IEEE Trans Biomed Eng* 37(9):837–843
 62. Tripathy R, Sharma L, Dandapat S (2016) Detection of shockable ventricular arrhythmia using variational mode decomposition. *J Med Syst* 40(4):79
 63. Unser M, Aldroubi A (1996) A review of wavelets in biomedical applications. *Proc IEEE* 84(4):626–638
 64. Yang H, Bukkapatnam ST, Komanduri R (2007) Nonlinear adaptive wavelet analysis of electrocardiogram signals. *Phys Rev E* 76:026214
 65. Yildirim O (2018) A novel wavelet sequence based on deep bidirectional LSTM network model for ECG signal classification. *Comput Biol Med* 96:189–202
 66. Yildirim O, Baloglu U (2018) Heartbeat type classification with optimized feature vectors. *Int J Optim Control Theories Appl* 8(2):170–175
 67. Yildirim O, Plawiak P, Tan RS, Acharya R (2018) Arrhythmia detection using deep convolutional neural network with long duration ECG signals. *Comput Biol Med* 102:411–420
 68. Yildirim O, Tan RS, Acharya UR (2018) An efficient compression of ecg signals using deep convolutional autoencoders. *Cogn Syst Res* 52:198–211. <https://doi.org/10.1016/j.cogsys.2018.07.004>
 69. Zadeh LA (1996) Fuzzy sets. In: Klir GJ (ed) Fuzzy sets, fuzzy logic, and fuzzy systems: selected papers by Lotfi A Zadeh. World Scientific, Singapore, pp 394–432
 70. Zala J, Sharma M, Bhalerao R (2018) Tunable q-wavelet transform based features for automated screening of knee-joint vibroarthrographic signals. In: 2018 5th international conference on signal processing and integrated networks (SPIN), pp 348–352. <https://doi.org/10.1109/SPIN.2018.8474117>
 71. Zhang XS, Zhu YS, Thakor NV, Wang ZZ (1999) Detecting ventricular tachycardia and fibrillation by complexity measure. *IEEE Trans Biomed Eng* 46(5):548–555

Publisher's Note Springer Nature remains neutral with regard to jurisdictional claims in published maps and institutional affiliations.